Theoretical Prediction of a Time-Reversal Broken Chiral Superconducting Phase Driven by Electronic Correlations in a Single TiSe$_2$ Layer

R. Ganesh,[1] G. Baskaran,[2,3] Jeroen van den Brink,[1,4] and Dmitry V. Efremov[1]

[1]*Institute for Theoretical Solid State Physics, IFW-Dresden, D-01171 Dresden, Germany*
[2]*The Institute of Mathematical Sciences, CIT Campus, Chennai 600 113, India*
[3]*Perimeter Institute for Theoretical Physics, Waterloo, Ontario, Canada N2L 2Y5*
[4]*Department of Physics, TU Dresden, D-01062 Dresden, Germany*

Bulk TiSe$_2$ is an intrinsically layered transition metal dichalcogenide hosting both superconducting and charge-density-wave ordering. Motivated by the recent progress in preparing two-dimensional transition metal dichalcogenides, we study these frustrated orderings in a single trilayer of TiSe$_2$. Using a renormalization group approach, we find that electronic correlations can give rise to charge-density-wave order and two kinds of superconductivity. One possible superconducting state corresponds to unconventional s_{+-} pairing. The other is particularly exciting as it is chiral, breaking time-reversal symmetry. Its stability depends on the precise strength and screening of the electron-electron interactions in two-dimensional TiSe$_2$.

Introduction.—Transition metal dichalcogenides (TMDs) with the chemical formula MX_2, where M is a transition metal from groups IV-VI (Ti, Zr, Hf, V, Nb, Ta, etc.) and X is a chalcogen element (Se, S, Te), are emerging as a new class of two-dimensional materials with high potential for nanoelectronics applications [1–4]. The intense research activity in this field is inspired by the graphene boom, driven by the possibility of manufacturing a purely two-dimensional material with high carrier mobility. TMDs consist of stacked X-M-X trilayers which, like graphene, have hexagonal symmetry. These trilayers are held together by weak van der Waals forces, which allows exfoliation of the individual trilayers and deposition onto various substrates [5].

TMDs display a rich variety of ordering phenomena. Metallic TMDs have a generic instability towards the formation of different types of charge-density waves (CDWs), some also host superconductivity (SC). Because of the presence of transition metal elements, electron-electron interactions may play a significant role here, giving us a highly interesting mix of ingredients. It is well known that the competition of SC with density waves in the presence of electronic correlations may lead to unconventional superconducting order, particularly in lower-dimensional systems. Commonly suggested examples are d-wave pairing in quasi-2D cuprate superconductors [6], s_{+-} pairing in layered iron pnictides [7,8], and p-wave triplet pairing in Sr$_2$RuO$_4$ [9]. Ordering in these materials remains under debate with several other proposals (e.g., Refs. [10–12]).

Sr$_2$RuO$_4$ is particularly interesting as its superconductivity may be characterized by a *chiral* order parameter that spontaneously breaks time-reversal symmetry [13], a property it shares with just a few other very low temperature SCs, e.g., UPt$_3$ [14] and (TMTSF)$_2$PF$_6$ [15]. Ordering which breaks time reversal has also been discussed in the context of cuprates [16] and Na$_x$CoO$_2$ · yH$_2$O [17,18]. Vortices in these chiral SCs harbor Majorana fermions [19], which may constitute the building blocks needed for future quantum computing technologies, robust against decoherence [20].

We focus on frustrated superconductivity in TiSe$_2$, which in bulk form is a layered semimetal with a CDW transition at ∼200 K [21,22]; it has recently emerged that the CDW order has chiral character [23–26]. Upon intercalation with copper, the CDW melts and nodeless SC appears with a critical temperature $T_c \approx 4$ K [27,28]. In this Letter, we consider a single trilayer of TiSe$_2$ and show that it hosts exciting ordering phenomena. Using a renormalization group (RG) approach, we show that the melting of CDW order gives way to one of two possible superconducting ground states, both of which are unconventional. The first is a time-reversal invariant (TRI) state with s_{+-} pairing while the other corresponds to time-reversal-breaking (TRB) chiral SC; see Fig. 1. Their relative stability depends on the precise strength and screening of the electron-electron interactions in a 2D trilayer of TiSe$_2$ deposited on some substrate.

Effective Lagrangian and couplings.—We performed *ab initio* calculations using FPLO (full-potential local-orbital minimum-basis code) [29,30] to find the Fermi surfaces of a single TiSe$_2$ trilayer. In line with previous reports [31], we find (i) two holelike pockets around the Γ point which are nearly degenerate and (ii) three electron-like pockets, one around each M point in the Brillouin zone. In the 3D case, these bands become elongated along the Z axis and form distorted cylinders—the 3D material has an additional spherical pocket around the Γ point.

Ab initio Fermi surfaces show approximate nesting between electron and hole pockets, which leads to
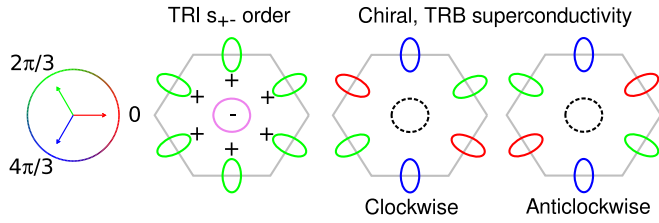
FIG. 1 (color online). Unconventional superconducting orders in a single trilayer of TiSe2. From left to right: Color map representing superconducting phase, time-reversal-invariant (TRI) s_{+-} ordering, and clockwise and anticlockwise variants of chiral, time-reversal-broken (TRB) ordering.

FIG. 2 (color online). Representative umklapp scatterings allowed by the geometry of TiSe2. They arise from the symmetry properties of the M points, viz., $\vec{M}_1 + \vec{M}_2 + \vec{M}_3 = 0$ and $2\vec{M}_i \equiv 0$.

logarithmic singularities in both particle-particle and particle-hole channels. In order to treat these on an equal footing, we use RG analysis to find the low energy couplings. There is, in fact, good nesting at energies above the Fermi level where our RG procedure operates.

In the following RG analysis, we approximate the band structure as follows. We merge the two hole pockets around the Γ point and give it the band index 0. We associate the

indices $\alpha = 1, 2, 3$ with the three electron pockets around the M points. The electron and hole pockets are approximately nested, so that there are nine different scattering processes, U_1–U_9, allowed by momentum conservation (see Supplemental Material for a diagrammatic representation [32]). As the Fermi surfaces have small radii, these couplings can be taken as independent of the precise initial and final momenta. The system is described by the Lagrangian

$$\mathcal{L} = \psi_0^\dagger(\partial_\tau - \varepsilon_{0k})\psi_0 + \sum_{\alpha=0}^{3}\psi_\alpha^\dagger(\partial_\tau - \epsilon_{\alpha k})\psi_\alpha - \left\{ U_6(\psi_0^\dagger\psi_1^\dagger\psi_2\psi_3 + \psi_0^\dagger\psi_1^\dagger\psi_3\psi_2 + \text{cyclic exchange}) \right.$$

$$+ \frac{1}{2}U_4\psi_0^\dagger\psi_0^\dagger\psi_0\psi_0 + \sum_{\alpha=1}^{3}\left[U_1\psi_0^\dagger\psi_\alpha^\dagger\psi_\alpha\psi_0 + U_2\psi_0^\dagger\psi_\alpha^\dagger\psi_0\psi_\alpha + \frac{1}{2}U_3(\psi_0^\dagger\psi_0^\dagger\psi_\alpha\psi_\alpha + \text{H.c.}) + \frac{1}{2}U_5\psi_\alpha^\dagger\psi_\alpha^\dagger\psi_\alpha\psi_\alpha \right]$$

$$\left. + \frac{1}{2}\sum_{\alpha\neq\beta}[U_7\psi_\alpha^\dagger\psi_\beta^\dagger\psi_\beta\psi_\alpha + U_8\psi_\alpha^\dagger\psi_\beta^\dagger\psi_\alpha\psi_\beta + U_9\psi_\alpha^\dagger\psi_\alpha^\dagger\psi_\beta\psi_\beta] \right\}. \tag{1}$$

We have implicitly assumed the spin structure $\sigma\sigma'\sigma'\sigma$; e.g., $U_2\psi_0^\dagger\psi_\alpha^\dagger\psi_0\psi_\alpha = \sum_{\sigma\sigma'}U_2\psi_{\sigma0}^\dagger\psi_{\sigma'\alpha}^\dagger\psi_{\sigma'0}\psi_{\sigma\alpha}$. For nested hole and electron pockets, the dispersions reduce to $(-)\epsilon_{0k} \approx \epsilon_{1k+M_1} = (k_x^2 + k_y^2)/2m - \mu$. There are three allowed umklapp processes: U_3, U_6, and U_9, as depicted in Fig. 2. We emphasize that U_6 has no analog in other multiband systems considered within RG recently, neither in pnictides [33,34] nor in graphene [35,36]. In pnictides, graphene, or even in the cuprates, RG flow gives low energy couplings that are conducive to SDW order [33,35,37]. In TiSe2, however, CDW order arises although the microscopic interactions are repulsive. We later show that it is precisely the U_6 umklapp term that drives CDW as opposed to SDW order.

RG flow proceeds by integrating out excitations above a floating cutoff scale. Because of approximate nesting, the electron-hole polarization bubble [$|\Pi_{\text{el-h}}| \propto (N/2)\log(\Lambda/\max\{T,\mu_d\})$] has the same logarithmic divergence as the particle-particle bubble [$C_{\text{h-h}} = C_{\text{el-el}} \propto (N/2)\log(\Lambda/T)$]. We use conventional one-loop RG keeping only logarithmically divergent terms given by parquet diagrams. The flow of couplings is given by

$$\dot{u}_1 = u_1^2 + u_3^2 - 2u_6^2,$$
$$\dot{u}_2 = -2u_2^2 - 2u_6^2 + 2u_2u_1,$$
$$\dot{u}_3 = u_3\{4u_1 - 2u_2 - u_4 - u_5 - 2u_9\},$$
$$\dot{u}_4 = -u_4^2 - 3u_3^2,$$
$$\dot{u}_5 = -u_3^2 - u_5^2 - 2u_9^2,$$
$$\dot{u}_6 = u_6\{2u_1 - u_2 + u_3 - u_7 - u_8\},$$
$$\dot{u}_7 = 2u_6^2 - u_7^2 - u_8^2,$$
$$\dot{u}_8 = -2u_7u_8,$$
$$\dot{u}_9 = -u_3^2 + 2u_6^2 - 2u_5u_9 - u_9^2. \tag{2}$$

The derivative is with respect to RG time $t = \log(W/E)$, where W is the bandwidth and E is the floating RG scale. In addition, we have scaled the interaction amplitudes U_i by the DOS at the Fermi level N_i ($u_i \equiv N_iU_i$). The derivation for u_5 is illustrated in the Supplemental Material [32]; others can be derived similarly. These parquet equations are valid for the energy $E \gtrsim \mu$. Below this energy, density-wave channels and superconductivity decouple and the flow has to be modified [38]. In this

Letter, we consider small Fermi pockets, thus neglecting the change of flow at $E \sim \mu$.

Ordering instabilities.—We introduce infinitesimal test vertices in particle-hole and particle-particle channels:

$$\delta\mathcal{L}_{\text{CDW}} = \sum_{\alpha=1}^{3} \rho_{c\alpha}^{(0)} \sigma_{\eta\eta'}^{0} \psi_{0\eta}^{\dagger} \psi_{\alpha\eta'},$$

$$\delta\mathcal{L}_{\text{SDW}} = \sum_{\alpha=1}^{3} \rho_{s\alpha}^{(0)} \sigma_{\eta\eta'}^{x} \psi_{0\eta}^{\dagger} \psi_{\alpha\eta'},$$

$$\delta\mathcal{L}_{\text{SC}} = \Delta_{0}^{(0)} i\sigma_{\eta\eta'}^{y} \psi_{0\eta}^{\dagger} \psi_{0\eta'}^{\dagger} + \sum_{\alpha=1}^{3} \Delta_{\alpha}^{(0)} i\sigma_{\eta\eta'}^{y} \psi_{\alpha\eta}^{\dagger} \psi_{\alpha\eta'}^{\dagger},$$

where σ^0 and σ^α are the identity and the Pauli matrices, respectively. We suppose implicit summation over the spin index. Writing the gap equation for each order, we identify a corresponding "effective vertex" as a function of u_α couplings (see Supplemental Material [32]). Within this analysis in the framework of the linear approximation, the CDW and SDW orders at each M point decouple. Furthermore, at each M point, both CDW and SDW order parameters decouple into two parts, which we designate "real" and "imaginary." They obey, correspondingly, $(\rho_{c/s,\alpha}^{r})^* = +\rho_{c/s,\alpha}^{r}$ and $(\rho_{c/s,\alpha}^{i})^* = -\rho_{c/s,\alpha}^{i}$. The effective vertices for real and imaginary SDW and CDW orders are given by $\Gamma_{\text{real or imag}}^{\text{SDW}} = u_1 \pm u_3$, $\Gamma_{\text{real or imag}}^{\text{CDW}} = u_1 \mp u_3 - 2u_2$. The RG procedure gives the first instability when coming down from a high temperature disordered phase, corresponding to single-Q CDW or SDW order. This is consistent with experiments on 3D TiSe$_2$ where single-Q order occurs at $T_{\text{CDW},1} \sim 200$ K, followed by multiple-Q order at a lower $T_{\text{CDW},2} \sim 186$ K [23,25].

In the superconducting channel, however, our Fermi surface geometry couples the order parameters on individual pockets. In accord with symmetry considerations, we get four eigenmodes of superconductivity. (i) s_{++} conventional superconductivity, characterized by real order parameters on the central pocket ($\Delta_0 = \Delta_\Gamma$) and the pockets around M points ($\Delta_1 = \Delta_2 = \Delta_3 = \Delta_M$), both having the same sign [$\text{sgn}(\Delta_\Gamma) = \text{sgn}(\Delta_M)$]. (ii) s_{+-} with real order parameters having different signs on the central and M pockets, i.e., [$\text{sgn}(\Delta_0) = -\text{sgn}(\Delta_M)$], as shown in Fig. 1. It is analogous to the order parameter proposed for the recently discovered Fe-based superconductors. (iii),(iv) Chiral superconductivity, which breaks time-reversal symmetry. At the level of linearized gap equations, the central pocket is completely decoupled with no pairing. The M pockets order in one of two degenerate solutions, corresponding to clockwise and anticlockwise winding of the phase of the order parameters, shown in Fig. 1. One of the two solutions is given by $\Delta_1 = e^{i2\pi/3}\Delta_2 = e^{-i2\pi/3}\Delta_3 = \Delta_M$. A similar phase has been proposed in highly doped graphene [35,36,39–41] and MgCNi$_3$ [42]. The effective vertices are given
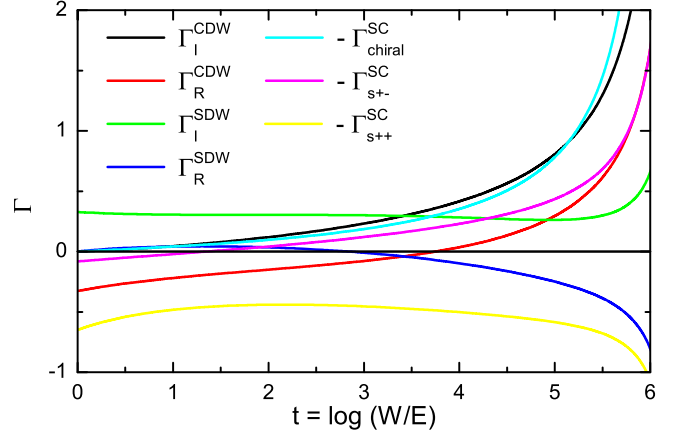
FIG. 3 (color online). RG flow of effective vertices. We have used bare interactions estimated assuming intra-atomic Coulomb interactions: $u_1^{(0)} = u_2^{(0)} = u_3^{(0)} = 0.82u^{(0)}$, $u_4^{(0)} = 1.85u^{(0)}$, $u_5^{(0)} = u_7^{(0)} = u_8^{(0)} = u_9^{(0)} = 0.6u^{(0)}$, and $u_6^{(0)} = 0.675u^{(0)}$, taking $u^{(0)} = 0.2$. Chiral SC eventually dominates.

by $-\Gamma_{s_{++}}^{\text{SC}} = -(u_4 + u_5 + 2u_9)/2 - \text{sgn}(u_3)R$, $-\Gamma_{s_{+-}}^{\text{SC}} = -(u_4 + u_5 + 2u_9)/2 + \text{sgn}(u_3)R$, $-\Gamma_{\text{chiral}}^{\text{SC}} = -u_5 + u_9$, where we have denoted $R = \sqrt{12u_3^2 + (u_4 - u_5 - 2u_9)^2}/2$.

Before analyzing RG flow, we consider "bare interactions" at mean-field level. As interactions are dominated by intra-atomic Coulomb repulsion, the bare couplings are proportional to the partial contributions of Ti t_{2g} and Se p orbitals to DOS at the Fermi pockets. From *ab initio* calculations, we find orbital contributions to states in each Fermi pocket to be $N_{\text{Ti}}^{\Gamma} \sim 0.8$, $N_{\text{Se}}^{\Gamma} \sim 1.1$, $N_{\text{Ti}}^{M} \sim 0.75$, and $N_{\text{Se}}^{M} \sim 0.2$. We can now estimate the bare interactions, e.g., $u_1^{(0)} = u^{(0)}(N_{\text{Ti}}^{\Gamma}N_{\text{Ti}}^{M} + N_{\text{Se}}^{\Gamma}N_{\text{Se}}^{M})$, $u_4^{(0)} = u^{(0)}(\{N_{\text{Ti}}^{\Gamma}\}^2 + \{N_{\text{Se}}^{\Gamma}\}^2)$, where $u^{(0)}$ is a parameter capturing the strength of the Coulomb interaction. Using these values, we find that the largest effective vertex corresponds to real SDW order $\Gamma_{\text{real}}^{\text{SDW}} \sim (0.33)u^{(0)}$. Superconducting channels drop out as their effective vertices are repulsive. Mean-field treatment thus predicts SDW order; however, RG flow modifies the couplings and changes the preferred ordering. Figure 3 shows the RG flow of effective vertices starting from these bare interactions; chiral SC ultimately dominates.

Fixed points in the RG flow.—The flow of couplings given by Eq. (2) is governed by three fixed points, wherein all couplings scale with with one diverging quantity. We rewrite the interactions as $u_i = b_i u$, with $u > 0$ being the divergent scale. The three fixed points are as follows.

(i) CDW fixed point: $b_2 = -1$, with all other couplings negligible, $b_{i\neq 2} = 0$. At this fixed point, the largest effective vertices correspond to both real and imaginary solutions of CDW order, $\Gamma_{\text{real}}^{\text{CDW}} = \Gamma_{\text{imag}}^{\text{CDW}}$.

(ii) Chiral SC fixed point: $b_9 = -b_5/2 > 0$, while other b's vanish. The largest effective vertex then corresponds to chiral SC.
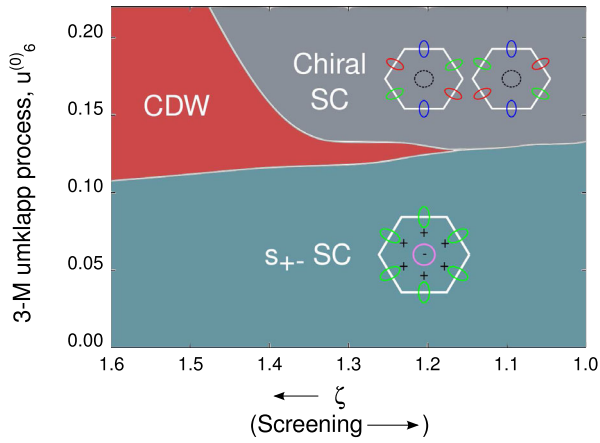
FIG. 4 (color online). The basins of the three fixed points. The bare vertices are $u_1^{(0)}/\zeta = u_2^{(0)} = u_3^{(0)} = 0.82u^{(0)}/\zeta$, $u_4^{(0)} = 1.85u^{(0)}$, $u_5^{(0)}/\zeta = u_7^{(0)}/\zeta = u_8^{(0)} = u_9^{(0)} = 0.6u^{(0)}/\zeta$. The precise location of basin boundaries weakly depends on $u^{(0)}$.

(iii) s_{+-} fixed point: $b_4 = -1$, $b_3 = \sqrt{5/11}$, $b_1 = 1/11$, $b_5, b_9 = -1/3$. The couplings b_2, b_6, b_7, b_8 vanish. The leading vertex is s_{+-} SC.

We emphasize a key difference *vis-à-vis* phonon-driven ordering: a phonon mechanism would suggest CDW order and s_{++} pairing. In contrast, electronic correlations give CDW order and s_{+-} or chiral SC. The absence of s_{++} order can be traced to the flow equation for u_3 in Eq. (2). The sign of u_3 cannot change under RG flow and always remains positive, thus favoring s_{+-} pairing over s_{++}.

Phase diagram in RG scheme.—RG flow crucially depends on bare values of couplings, which we estimate from *ab initio* data for orbital DOS. Building upon this, we introduce two free parameters, u_6^0 and ζ, to characterize the bare couplings. The parameter u_6^0 is simply the bare value of the u_6 coupling; we use it as a parameter to emphasize the key role of the u_6 process. The second parameter ζ models the momentum dependence of the screened Coulomb interaction. The low energy scattering processes fall into two classes: small and large ($\sim M$) momentum transfer. The latter are reduced by the factor ζ. For example, we have $u_1^{(0)} = u^{(0)}(N_{Ti}^\Gamma N_{Ti}^M + N_{Se}^\Gamma N_{Se}^M)$ and $u_2^{(0)} = u^{(0)}(N_{Ti}^\Gamma N_{Ti}^M + N_{Se}^\Gamma N_{Se}^M)/\zeta$. For strong screening, we expect local interactions and momentum-independent interactions, giving $\zeta \sim 1$. For weak screening, $\zeta > 1$.

Figure 4 shows the fate of RG flow as a function of these two parameters. The crucial role of hexagonal symmetry can be seen by examining the line $u_6^0 = 0$. When the bare value of u_6 is zero, RG flow cannot generate a finite u_6 value [see Eq. (2)]. Without u_6 (along the $u_6^0 = 0$ line), we do not approach the CDW fixed point or the chiral SC fixed point. To estimate the "microscopic" value of u_6^0, we could use the same reasoning as with the other bare parameters to

obtain $u_6^{bare}(\zeta) = \{(N_{Se}^\Gamma)^{1/2}(N_{Se}^M)^{3/2} + (N_{Ti}^\Gamma)^{1/2}(N_{Ti}^M)^{3/2}\}/\zeta$. As u_6 involves large momentum transfer, it is scaled down by ζ. This choice of u_6 places us in the basins of CDW and s_{+-} fixed points. However, for some ζ values, the microscopic parameters lie very close to the border of the chiral SC basin. Taken together, our results suggest that 2D TiSe$_2$ may host CDW order, chiral superconductivity, or s_{+-} pairing.

Discussion.—We analyzed the competing phases in two-dimensional hexagonal structures which allow special umklapp processes. In systems with Coulomb repulsion, these processes give rise to CDW order instead of SDW. This CDW state competes with chiral and s_{+-} superconductivity and *not* s_{++} superconductivity expected from a phonon mechanism. We focused on two-dimensional TiSe$_2$ with two small hole pockets around Γ and electron pockets around the M points. This physics could also appear in 2D TiS$_2$ and other materials with similar band structure. Our results may also be relevant for layered 3D TiSe$_2$, which has an additional spherical hole pocket around the Γ point—our RG analysis is still valid at high energies when the bands are 2D-like. While nodeless superconductivity has been seen in 3D TiSe$_2$ [27,28], our results call for a more detailed examination of the nature of superconductivity, particularly in exfoliated layers with nanoscopic thicknesses. Earlier works have attempted to explain CDW ordering in 3D TiSe$_2$ invoking excitons [43], the band Jahn-Teller effect [44], and orbital ordering [45]; our RG analysis may provide a unified explanation for CDW and SC orders.

Our results for TiSe$_2$ should be compared with the pnictides wherein Coulomb interactions lead to s_{+-} SC order which competes with SDW order. The different behavior of TiSe$_2$ ultimately stems from u_6, the umklapp process allowed by the geometry of the M pockets. For CDW to win over SDW order, we require a negative value of u_2 at the fixed point, whereas the bare Coulombic value of u_2 is positive. A nonzero u_6 plays a key role here by reducing the value of u_2 under RG flow [see Eq. (2)] to negative values, similar to the role of interchain coupling in coupled 1D chains [46].

The proposed chiral SC order has many interesting implications. Previous studies have highlighted the possibility of fractional vortices connected by domain walls [47]. If the central pocket is indeed decoupled as shown in Fig. 1, this pocket may undergo pairing with a different transition temperature. Alternatively, higher order couplings may kick in and induce chiral order in the central pocket. This possibility is favored by *ab initio* calculations: each M pocket is dominated by a single Ti t_{2g} orbital while the central pocket shows a strong angular dependence in t_{2g} orbital character. If the central pocket were to inherit pairing by a proximity effect driven by local orbital-centered interactions, we may obtain $d_{x^2-y^2} + id_{xy}$ pairing.

[1] M. Xu, T. Liang, M. Shi, and H. Chen, Chem. Rev. **113**, 3766 (2013).

[2] B. Radisavljevic and A. Kis, Nat. Mater. **12**, 815 (2013).

[3] H. Terrones, F. López-Urías, and M. Terrones, Sci. Rep. **3**, 1549 (2013).

[4] Q. H. Wang, K. Kalantar-Zadeh, A. Kis, J. N. Coleman, and M. S. Strano, Nat. Nanotechnol. **7**, 699 (2012).

[5] J. N. Coleman, M. Lotya, A. O'Neill, S. D. Bergin, P. J. King, U. Khan, K. Young, A. Gaucher, S. De, R. J. Smith *et al.*, Science **331**, 568 (2011).

[6] C. C. Tsuei and J. R. Kirtley, Rev. Mod. Phys. **72**, 969 (2000).

[7] I. I. Mazin, D. J. Singh, M. D. Johannes, and M. H. Du, Phys. Rev. Lett. **101**, 057003 (2008).

[8] I. Mazin and J. Schmalian, Physica (Amsterdam) **469C**, 614 (2009).

[9] A. P. Mackenzie and Y. Maeno, Rev. Mod. Phys. **75**, 657 (2003).

[10] Q. Li, Y. N. Tsay, M. Suenaga, R. A. Klemm, G. D. Gu, and N. Koshizuka, Phys. Rev. Lett. **83**, 4160 (1999).

[11] E. Wang, H. Ding, A. V. Fedorov, W. Yao, Z. Li, Y.-F. Lv, K. Zhao, L.-G. Zhang, Z. Xu, J. Schneeloch *et al.*, Nat. Phys. **9**, 621 (2013).

[12] K. Machida and M. Ichioka, Phys. Rev. B **77**, 184515 (2008).

[13] C. Kallin and A. J. Berlinsky, J. Phys. Condens. Matter **21**, 164210 (2009).

[14] G. R. Stewart, Z. Fisk, J. O. Willis, and J. L. Smith, Phys. Rev. Lett. **52**, 679 (1984).

[15] D. Jérome, A. Mazaud, M. Ribault, and K. Bechgaard, J. Phys. (Paris), Lett. **41**, 95 (1980).

[16] R. B. Laughlin, Phys. Rev. Lett. **80**, 5188 (1998).

[17] G. Baskaran, Phys. Rev. Lett. **91**, 097003 (2003).

[18] D. Sa, M. Sardar, and G. Baskaran, Phys. Rev. B **70**, 104505 (2004).

[19] D. A. Ivanov, Phys. Rev. Lett. **86**, 268 (2001).

[20] C. Nayak, S. H. Simon, A. Stern, M. Freedman, and S. Das Sarma, Rev. Mod. Phys. **80**, 1083 (2008).

[21] F. J. Di Salvo, D. E. Moncton, and J. V. Waszczak, Phys. Rev. B **14**, 4321 (1976).

[22] K. Rossnagel, J. Phys. Condens. Matter **23**, 213001 (2011).

[23] J. Ishioka, Y. H. Liu, K. Shimatake, T. Kurosawa, K. Ichimura, Y. Toda, M. Oda, and S. Tanda, Phys. Rev. Lett. **105**, 176401 (2010).

[24] J. Ishioka, T. Fujii, K. Katono, K. Ichimura, T. Kurosawa, M. Oda, and S. Tanda, Phys. Rev. B **84**, 245125 (2011).

[25] J.-P. Castellan, S. Rosenkranz, R. Osborn, Q. Li, K. E. Gray, X. Luo, U. Welp, G. Karapetrov, J. P. C. Ruff, and J. van Wezel, Phys. Rev. Lett. **110**, 196404 (2013).

[26] B. Zenker, H. Fehske, H. Beck, C. Monney, and A. R. Bishop, Phys. Rev. B **88**, 075138 (2013).

[27] E. Morosan, H. W. Zandbergen, B. S. Dennis, J. W. G. Bos, Y. Onose, T. Klimczuk, A. P. Ramirez, N. P. Ong, and R. J. Cava, Nat. Phys. **2**, 544 (2006).

[28] S. Y. Li, G. Wu, X. H. Chen, and L. Taillefer, Phys. Rev. Lett. **99**, 107001 (2007).

[29] K. Koepernik and H. Eschrig, Phys. Rev. B **59**, 1743 (1999).

[30] http://www.fplo.de.

[31] C. M. Fang, R. A. de Groot, and C. Haas, Phys. Rev. B **56**, 4455 (1997).

[32] See Supplemental Material at http://link.aps.org/supplemental/10.1103/PhysRevLett.113.177001 for a diagrammatic representation of scattering processes and for details about band structure, flow equations, effective vertices and the RG flow cutoff.

[33] A. V. Chubukov, D. V. Efremov, and I. Eremin, Phys. Rev. B **78**, 134512 (2008).

[34] R. Thomale, C. Platt, W. Hanke, and B. A. Bernevig, Phys. Rev. Lett. **106**, 187003 (2011).

[35] R. Nandkishore, L. S. Levitov, and A. V. Chubukov, Nat. Phys. **8**, 158 (2012).

[36] M. L. Kiesel, C. Platt, W. Hanke, D. A. Abanin, and R. Thomale, Phys. Rev. B **86**, 020507 (2012).

[37] A. T. Zheleznyak, V. M. Yakovenko, and I. E. Dzyaloshinskii, Phys. Rev. B **55**, 3200 (1997).

[38] S. Maiti and A. V. Chubukov, Phys. Rev. B **82**, 214515 (2010).

[39] A. M. Black-Schaffer and S. Doniach, Phys. Rev. B **75**, 134512 (2007).

[40] S. Pathak, V. B. Shenoy, and G. Baskaran, Phys. Rev. B **81**, 085431 (2010).

[41] R. Nandkishore, R. Thomale, and A. V. Chubukov, Phys. Rev. B **89**, 144501 (2014).

[42] K. Voelker and M. Sigrist, arXiv:cond-mat/0208367.

[43] C. Monney, C. Battaglia, H. Cercellier, P. Aebi, and H. Beck, Phys. Rev. Lett. **106**, 106404 (2011).

[44] Y. Yoshida and K. Motizuki, J. Phys. Soc. Jpn. **49**, 898 (1980).

[45] J. van Wezel, Europhys. Lett. **96**, 67011 (2011).

[46] P. A. Lee, T. M. Rice, and R. A. Klemm, Phys. Rev. B **15**, 2984 (1977).

[47] T. Yanagisawa, Y. Tanaka, I. Hase, and K. Yamaji, J. Phys. Soc. Jpn. **81**, 024712 (2012).